Hydraulic Resistance Modelling of the Porous Media Approaches for a Pool-type Sodium-cooled Fast Reactor

Churl Yoon*, Huee-Youl Ye, Jae Hyuk Eoh
Advanced Reactor Technology Development Division, Korea Atomic Energy Research Institute,
111 Daedeok-daero 989 Beon-gil, Yuseong-gu, Daejeon 34057, Korea
**E-mail: cyoon@kaeri.re.kr*

***Keywords :** sodium-cooled fast reactor (SFR) , SALUS, computational fluid dynamics (CFD), porous media approach, hydraulic resistance

1. Introduction

Korea Atomic Energy Research Institute (KAERI) has been developing a design and analysis technique for a pool-type sodium-cooled fast reactor called SALUS (Small, Advanced, Long-cycled and Ultimate Safe SFR), which would generate 100MWe with a long refueling period of around 20 years. SALUS is a pool-type SFR (Sodium-cooled Fast Reactor) including two pumps, four IHXs (Intermediate Heat Exchangers), and four DHXs (Decay Heat Exchangers).[1] These IHXs and DHXs are shell-and-tube type counter-current flow sodium-to-sodium heat exchangers.

CFD (Computational Fluid Dynamics) analyses[2] were performed to get the fluid flow field and temperature distribution over the PHTS (Primary Heat Transfer System) being directly contact with HAA (Head Access Area) and RVCS (Reactor Vault Cooling System), for developing and verifying the SALUS design. Figure 1 shows side- and top-views of the SALUS PHTS (Primary Heat Transfer System) Assembly. In the CFD modelling, the secondary loops of the 4 IHXs and 4 DHXs were ommitted and the shell-side tube bundles which PHTS sodium flows across were approximated as porous media having proper hydraulic resistances and heat removal rates. UIS (Upper Internal Structure) contains nine control rod guide tubes, hundreds of thermal couple lines and other guide tubes, the fluid flows regions inside which are also approximated as porous media. A commercial CFD software vended by Siemens Corp., STAR-CCM+ Version 16.02[3], was used for the CFD analyses.

In this study, a hydraulic resistance model of the porous media approaches for the SALUS IHXs, DHXs, and UIS were implemented into the CFD tool and verified by using experiment and calculation results. The verified hydraulic resistance models would be applied to the CFD analysis of SALUS PHTS.

2. Porous Media Approaches for the Shell-side of Heat Exchangers and inside the UIS

In the CFD analyses of SALUS PHTS, the shell-side tube bundles inside the SALUS IHXs and DHXs are simplified as porous media having proper hydraulic resistances and heat removal rates. The hydraulic resistances experienced by the fluid flowing over the tube bundles were accounted for as source terms of the momentum equations.

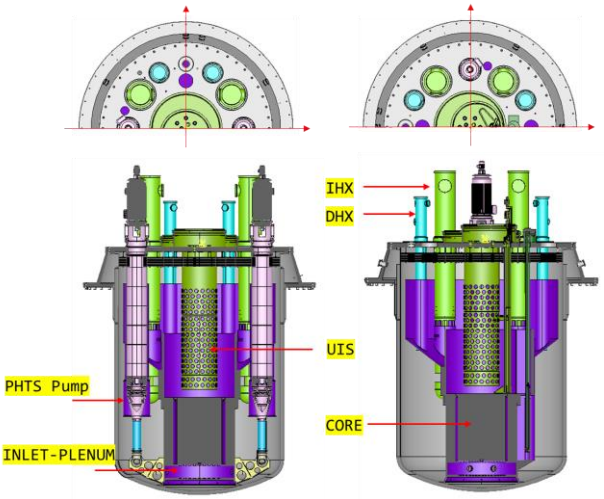

Fig. 1. SALUS PHTS assembly.

The assumptions in deriving the governing equations for the flows inside porous media are that the control volumes and the control surfaces are large relative to the interstitial spacing of the porous medium, and that the given control cells and control surfaces are assumed to contain both the fluid and the distributed solids. When one defines the volume porosity as $\gamma \equiv \frac{\mathrm{Vol_f}}{\mathrm{Vol_T}}$ and the area porosity as $\gamma_A \equiv \frac{A_f}{A_T}$, a direct application of the conservation principles gives the following continuity, momentum, and energy equations in a porous medium.[4]

$$\frac{\partial(\rho\gamma)}{\partial t}+\frac{\partial\left(\rho\gamma_A u_j\right)}{\partial x_j}=0 \tag{1}$$

$$\frac{\partial(\rho\gamma u_i)}{\partial t}+\frac{\partial\left(\rho\gamma_A u_j u_i\right)}{\partial x_j}=-\gamma_A\frac{\partial p}{\partial x_i}+\frac{\partial}{\partial x_j}\left[\mu_e\gamma_A\left(\frac{\partial u_i}{\partial x_j}+\frac{\partial u_j}{\partial x_i}\right)\right]+B_i-R_i \tag{2}$$

$$\frac{\partial(\rho\gamma H)}{\partial t}+\frac{\partial\left(\rho\gamma_A u_j H\right)}{\partial x_j}=\frac{\partial}{\partial x_j}\left(\Gamma_e\gamma_A\frac{\partial H}{\partial x_j}\right)+\gamma Q \tag{3}$$

Table 1: Thermal Design Parameters of the SALUS HXs

Parameter	IHX	DHX
Number of units	4	4
Rated heat removal capacity per unit	97.8 MW_t	1.67 MW_t
Number of tubes per unit	1050	114
Total tube length	4.85 m	2.13 m
Shell-side inlet temp.	510 ºC	360 ºC
Shell-side outlet temp.	357.7 ºC	251.1 ºC
Shell-side sodium flowrate	341.4 kg/s	11.74 kg/s
Heat transfer tube outer diameter	17.9 mm	21.7 mm
Pitch-to-diameter ratio	1.5	1.5
Heat transfer tube material	9Cr-1Mo-V	9Cr-1Mo-V
Number of tube support structure (axially)	5	2

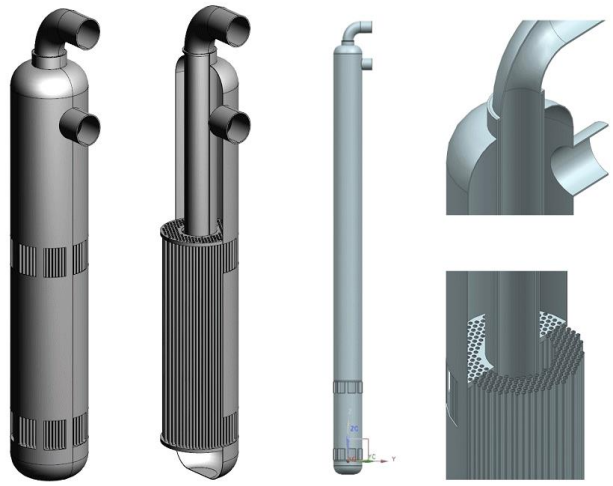

Fig. 2. Schematic design of the SALUS DHX.

Here, ρ, u, t, x, H, μ_e, and Γ_e are respectively density, velocity, time, distance, total energy, effective viscosity, and effective thermal diffusivity. B, R, and Q are defined as a body force, resistance to the flow in the porous media, and a heat source or sink, respectively.

When the cross-sectional views of a porous medium are uniform in an axial direction as like a tube bank, one can assume $\gamma = \gamma_A$ in the governing equations (1) ~ (3). Then, substituting $\gamma \cdot u$ with u^S, equations (1) ~ (3) become the general governing equations for u^S. The superficial velocity $u^S(=\gamma \cdot u)$ is an artificial flow velocity that assumes that only fluid passes the cross-sectional area and neglects the solid portion of the porous medium.[3]

The hydaulic resistance in the porous medium, R, in equation (2) consists of the viscous (linear) and the inertial (quadratic) resistance terms.

$$R_i = -\frac{\Delta P}{\Delta L}\Big)_i = \frac{\mu}{K} u_i^S + K_{loss} \frac{\rho}{2} u_i^S \left|U^S\right| \qquad (4)$$

Here, μ, K, and K_{loss} are respectively dynamic viscosity, permeability, and pressure loss coefficient. The first term in the right-hand side of equation (4) corresponds to Darcy's law for the flows in fluidized beds, which was deactivated in this study.

In Siemens STAR-CCM+, the turbulence transport equations are not solved in the porous regions.[3] Even though the effect of a porous region on turbulent flow depends on its internal structure, the real shape of a structure is not conserved and solids are assumed to be distributed over a porous region uniformly in the porous media approaches. Therefore, if turbulent properties are required in the porous region, users must specify directly turbulent parameters such as turbulence intensity and length scale, etc. In this study, turbulence models were not accounted for in the porous regions and the basic k-ε turbulence model was adopted when the channel flows containing the porous region becomes turbulent.

3. Hydraulic Resistance Model for Porous Media

In this section, the way how to implement the hydraulic resistance of the assumed porous media into momentum source terms in the CFD tool is tested and verified against available experimental data and correlations. Since the input forms of momentum source terms for hydraulic resistance could be varing depending on the CFD softwares brand, versions, and selected options, verification procedures of the cross(lateral) and axial hydraulic resistances to tube bundles were performed to confirm proper usage of the given CFD tool for porous media approaches. Additionally, implementation of the hydraulic resistances in the porous media approach for the lowest support plate in the SALUS UIS was also tested and verified.

3.1 Hydraulic Resistance for Cross Flows

Figure 2 shows a schematic design of the SALUS DHX, the design concept of which is similar to the SALUS IHX. In the shell-and-tube type heat exchanger region, secondary sodium flows upward inside the heat transfer tubes and primary sodium flows downward parallel with the heat transfer tubes in the shell-side sodium flow path. After the heat transfers inside both the IHX and DHX tube bundle regions, primary sodium is discharged into the lower part of the cold sodium pool.

The pressure drop calculations can be made for a unit flow channel composed of circular rod bundles, which have a specific pitch-to-diameter(P/d) ratio with a triangular pitch layout as shown in Figure 3. Thermal design parameters of the IHX and DHX have been produced complying with the design requirements of the fluid system of 100 MWe SALUS, as sumarized in Table 1.

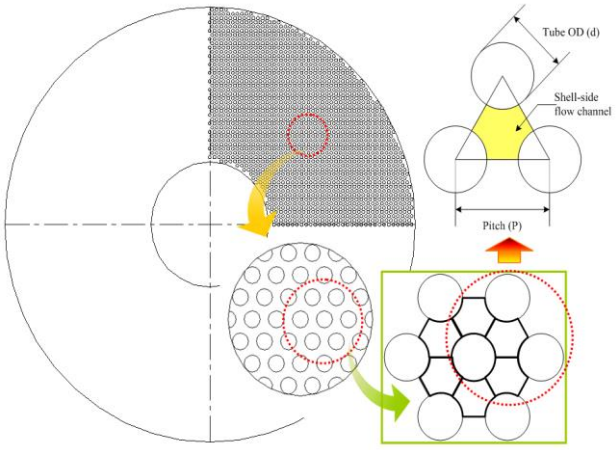

Fig. 3. Configuration of heat transfer tube array for the SALUS IHX and DHX.

For the verification of implementing the hydraulic resistances of the cross flows in the porous regions, a conventional experimental study by Derek B. Ebeling-Koning[5] was selected, which experimentally investigated the pressure drop across the inclined tube bundles. The test section was a duct with a rectangluar cross section of 142.875 x 28.575mm and a length of 914.4mm. Inside the duct, a tube bundle was installed with the pitch to diameter ratio (P/D) of 1.5 at 0, 30, 45, 90 degree inclinaions. Among all the test cases, the 90 degree inclination case was simulated first by using Siemens STAR-CCM+. The tubes with a diameter of 6.35mm were installed in in-line sqaure arrangment, so the hydraulic diameter becomes 10.3mm. The tested Reynolds number range was $1 \times 10^3 \sim 2.0 \times 10^4$, with water as a working fluid.

Zukauskas and Ulinskas[6] expressed the pressure drop through a tube banks by the Euler number, Eu.

$$\Delta P = Eu \frac{\rho u^2}{2} z \tag{5}$$

Here, z is the number of tube rows. Therefore, the hydraulic resistance term in the momentum equation becomes as follows:

$$\frac{\Delta P}{\Delta L} = Eu \frac{\rho u^2}{2} \frac{z}{\Delta L} = \frac{Eu}{pitch} \cdot \frac{\rho u^2}{2} \tag{6}$$

The equations of Eu for in-line tube banks with a pitch to diameter ratio (P/D) of 1.5 are expressed as,

$$\frac{Eu}{k_1} = \begin{cases} 0.263 + \dfrac{0.867\times10^2}{\mathrm{Re}} - \dfrac{0.202\times10}{\mathrm{Re}^2} & \text{for } 3 < \mathrm{Re} < 2\times10^3 \\ 0.235 + \dfrac{0.197\times10^4}{\mathrm{Re}} - \dfrac{0.124\times10^8}{\mathrm{Re}^2} & \\ \quad + \dfrac{0.312\times10^{11}}{\mathrm{Re}^3} - \dfrac{0.274\times10^{14}}{\mathrm{Re}^4} & \text{for } 2\times10^3 < \mathrm{Re} < 2\times10^6 \end{cases} \tag{7}$$

Here, $k_1 \approx 1.0$ for a square tube array.

For the CFD simulations, Euler number of Eq. (7) was implemented as a function of the simulated Reynolds number. The pressure loss rates were converted into the momentum source terms by using Eq. (6). At this time, note that the STAR-CCM+ users should be careful as entering the input values for the "Porous Inertial Resistance", since the required input value is a coefficient(multiplier) to a square of the superficial velocity at each location and in the unit of kg/m^4. The simulation results and the experimental data were summarized in Table 2. For the comparison, the normalized flow resistance components defined by D. B. Ebeling-Koning[5] were estimated as follows:

$$R_x^* \triangleq \frac{D_h^2}{\mu \left| \langle \underline{u} \rangle \right|} \frac{\Delta P_x}{L_x} \tag{8}$$

where, D_h and L_x are respectively hydraulic diameter and travelling distance in x-direction. And, the volume average velocity component is

$$\left| \langle \underline{u} \rangle \right| = \frac{\text{volumetric flow rate}}{\text{flow area}} \quad \left(= u^S \right)$$

Considering that the reported experimental error for the normalized flow resistance component R_x^* was ±5.1%, the simulation results show good agreement with the experimental data overally.

3.2 Hydaulic Resistance for Axial Flows through the Tube Bundle of Smooth Straight Pipes

Shell-side axial pressure losses of the straight tube bundle are mainly caused by the frictional loss on the tube outer surfaces. Since the pressure loss can be considered as a function of Reynolds numbers for an internal pipe flow, the hydraulic resistance in axial (Z-) direction can be calculated by simple Darcy friction factor[7] correlations.

$$f_z = \begin{cases} \dfrac{64}{\mathrm{Re}} & \text{for } \mathrm{Re} < 2{,}000 \\ \dfrac{1}{\left[1.8\log\left(\mathrm{Re}\right) - 1.64\right]^2} & \text{for } \mathrm{Re} > 4{,}000 \end{cases} \tag{9}$$

Where, Reynolds number is calculated by the internal pipe flow correlation of $Re = \rho u D/\mu$. Note that u here is the physical velocity, not superficial velocity. For shell-side sodium flow channel, the hydraulic diameter is defined as Eq. (10) by considering flow channel area.

$$A_f = \frac{\sqrt{3}}{4} P^2 - \frac{1}{2} \times \frac{\pi}{4} d_{o,w}^2$$

$$D_h = \frac{4A_f}{\pi d_{o,w} / 2} \tag{10}$$

where, A_f, P, $d_{o,w}$ and D_h denote flow channel area, pitch between tube centers, tube outer diameter, and shell-side hydraulic diameter, respectively. Then, the axial frictional pressure drop is obtained by the following equation.

$$\Delta P_{axial} = f_z \frac{L}{D_h} \cdot \frac{1}{2} \rho u_{axial}^2 \tag{11}$$

This pressure loss was also converted into a momentum source term as the same procedure in the previous section.

For the verification of the axial hydraulic resistance model, the rectangular channel flow with axial hydraulic resistances were simulated by the CFD tool. Since the design velocities of shell-side (bundle average) sodium flows for IHXs and DHXs at the full power operation conditions are about 1.05 and 0.214 m/s, respectively. Three sample velocities were selected in the range less than 1.0 m/s. The sodium density and dynamic viscosity were respectively set to be constant values of 847.4 kg/m^3 and 5.99×10^{-4} Pa·s at the sodium temperature of 400.0 °C. Table 3 summarizes the the comparison between the simulation and the calculation results, which proves that the shell-side axial hydraulic resistance along the tube bundle with triangular layout was properly implemented into the STAR-CCM+ CFD tool.

3.3 Hydaulic Resistance for the Flows through the UIS Lowest Support Plate

The upper internal structure (UIS) is used to guide and support several kinds of guide tubes. The UIS guides the core exit coolant to the intermediate heat exchanger, which is maintained at a uniform temperature by mixing. The UIS lowest support plate is the closest support plate right above the reactor core.

Fig. 4 presents the top view of the SALUS UIS (Upper Internal Structure) lowest support plate with a thickness of 30 mm. In the support plate, 172 flow holes with a diameter of 82.4 mm are installed in equal spacing between the CR (Control Rod), DM (Direct lifting Machine), sensing and thermal couple guide tubes. Since the design of the SALUS UIS lowest support plate has not fully determined yet, the plate was modelled as a porous medium in the STAR-CCM+ simulation except the CR and DM guide tube holes. The estimated porosity of the porous support plate is 0.228, as same as PGSFR. The pressure drop at the grid plate is modelled by the Diagram 3-12 in Idelchik[7] and Han[10], as follows.

$$\Delta P_{Grid} = K_i \frac{1}{2}\rho u^2 + \xi_{fr} \qquad (12)$$

$$\text{where } K_i = \frac{\Delta P}{\rho u_0^2 / 2} = \left(1.707 - \bar{f}\right)^2 \cdot \frac{1}{\bar{f}^2} \qquad (13)$$

Here, ξ_{fr} is the potential friction loss passing through the grid plate, u_o is flow velocity upstream, and $\bar{f}$ is the (actual flow area) to (frontal flow area) ratio.

The simple conceptual geometry was generated as shown in Figure 5(a), and the flow through a porous plate was simulated with a hydraulic resistance of Eq. (12). In this simple problem, the hydraulic resistance and the pressure drop across the porous plate can be estimated by hand calculations as follows.

Table 4: Simuation Input Values for the Porous Plate Flows

Input Parameter	Value
Inlet Velocity	1.0 m/s
Porosity	0.228
Y-Dir. Hydraulic Resistance	582092.8 kg/m^4
X- & Z-Dir. Hydraulic Resistance	1.0E+10 kg/m^4

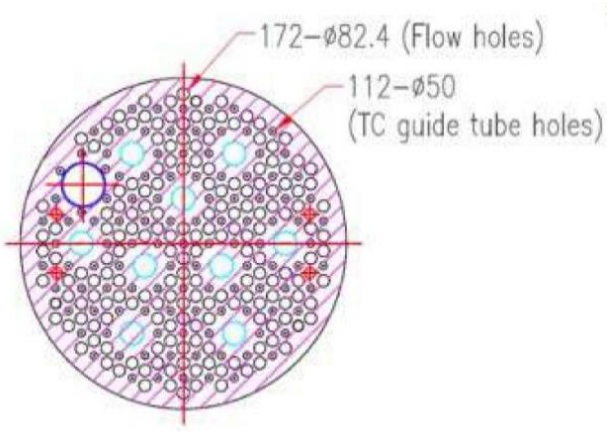

Fig. 4. Top view of the SALUS UIS lowest support plate.

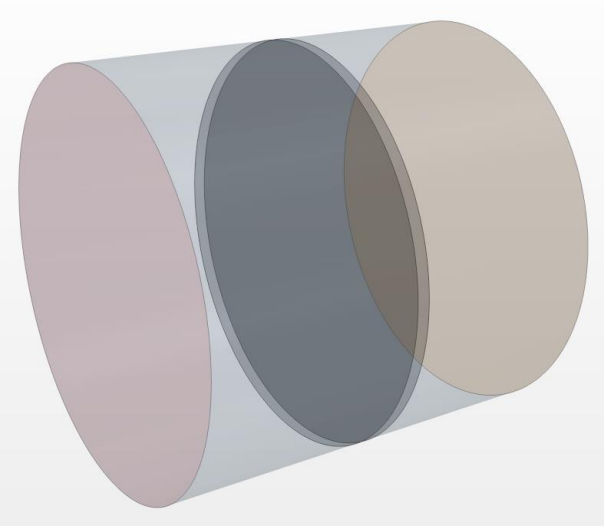

(a) Simple geometry for the CFD simulation

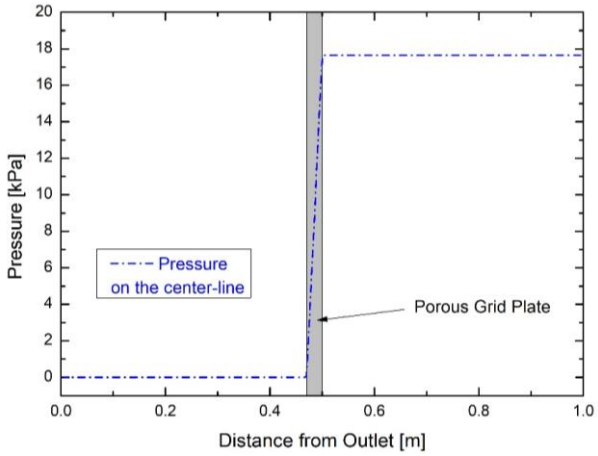

(b) Resultant pressure profile on the channel center line

Fig. 5. CFD simulation of the flow through a holed plate.

$$K_i = \frac{\Delta P}{\rho u_0^2 / 2} = \left(1.707 - 0.228\right)^2 \cdot \frac{1}{0.228^2} = 42.07912$$

The hydraulic reesistance term in the Y-momentum equation is calculated as

$$-R_Y = \frac{\Delta P_{Grid}}{\Delta L} = K \frac{\rho}{2\Delta L}\left(\beta V\right)^2$$
$$= 42.079 \frac{830 kg/m^3}{2\left(0.03m\right)}\left(\beta V\right)^2$$

where β is porosity.

Table 4 summarizes input parameters for the STAR-CCM+ simulation. The hydraulic resistance in orthogonal component to the flow direction were set as infinite large values. Finally, the pressure drops across the grid plate calculated as

$$\Delta P_{Grid} = K_i \frac{1}{2}\rho {u_0}^2 = \frac{42.079}{2}\left(830 kg/m^3\right)\left(1.0 m/s\right)^2,$$
$$= 17.4628 kPa$$

which is the same value as the simulation result as shown in Fig. 5(b). Therfore, it is concluded that the Idelchik' correlation (Eq. (12) & (13)) predicts the pressure drop across the grid plate properly.

4. Conclusions

In this study, hydraulic resistance models of the porous media approaches for SALUS CFD analyses have been established and verified by using experimental data and correlations. The followings are conclusions:

- For the lateral (cross) flow to a in-line tube bank, the hydraulic resistance correlation based on Euler number was adapted and implemented into the Siemens STAR-CCM+ CFD tool as a function of the local Reynolds number as well as the flow velocity. During this process, it was found that the STAR-CCM+ users should enter the input values for the "Porous Inertial Resistance" as a form of the coefficient (multiplier) to a square of the superficial velocity. Even thugh the simulation results show show good agreement with the experimental data [5] overally, any further validation efforts with experimental cross flow pressure drop data for triangular tube arrays might be needed to the completion.
- For the axial flows along smooth straight tube bundle, the hydraulic resistance in axial direction was implemented into the CFD tool by well-known Darcy friction factor correlations. The implemented hydraulic resistances were well verified by comparing the resultant pressure losses with the caulculations.
- For the pressure drop across a grid plate with equally-spaced flow holes, a correlation from Idelchik[7] was adapted. A conceptual problem was set for the CFD simulation for verification. And the simulation gave exactly the same value as the hand-calculated.

As a result, the methods to implement the hydraulic resistances for the porous media approaches in the SALUS CFD analyses were derived and verified.

In the future studies, the derived method shall be applied to a CFD simulation of a single IHX or DHX analysis and the results will be compared with those of a SFR heat exchanger design code called SHXSA[8]. For the future CFD analyses of SALUS PHTS, the measured pressure drop data by M. Kong et al.[9] will be utilized for establishing the more accurate hydraulic resistance models for the SALUS HXs in various operating conditions.

ACKNOWLEDGMENTS

This work was supported by the National Research Foundation of Korea (NRF) grant funded by the Korea government (MSIT). (No. 2021M2E2A1037871)

REFERENCES

[1] Ji-Woong Han, Dehee Kim, and Huee-Youl Ye, "Design Feasibility Study on DHRS for 100MWe Long Fuel Cycle Sodium-cooled Fast Reactor," KNS Spring Meeting, Jeju, 2022.
[2] Churl Yoon, Huee-Youl Ye, and Jae Hyuk Eoh, "CFD-Aided Design of a Small Modular SFR," KNS Autumn Meeting, Changwon, 2022.
[3] Siemens Corp., STAR-CCM+ Version 16.02.008: Theory Manual, 2021.
[4] N.E. Todreas and M.S. Kazimi, *Nuclear System II: Elements of Thermal Hydraulic Design*, Chap. 5, Hemisphere Publishing Corporation, 1990.
[5] Derek B. Ebeling-Koning, *Hydrodynamics of Single- and Two-Phase Flow in Inclined Rod Arrays*, Ph.D. Thesis, Massachusetts Institute of Technology, Feb. 1984.
[6] A Zukauskas and R. Ulinskas, "2.2.4 Banks of Plain and Finned Tubes," *Heat Exchanger Design Handbook: 1. Heat Exchanger Theory*, Hemisphere International Center for Heat and Mass Transfer, 1983.
[7] I.E. Idelchik, *Handbook of Hydraulic Resistance*, ACE-TR-6630, 1960.
[8] J.G. Han, "SHXSA 1.2 SVVR," KAERI Design Document, SAL-200-E2-472-001, 2021.
[9] M. Kong, W. S. Kim, H. J. Chung, H.S. Choi, J. Kim, T. H. Lee, and D.-J. Euh, "Experimental Identification of Pressure Drop Characteristics at the Shell Side of an Intermediate Heat Exchanger inside a Prototype Generation-IV Sodium-cooled Fast Reactor," *Nuclear Engineering and Design*, Vol. 348, pp. 177-186, 2019.

Table 2: Experimental and Simulation Results for the Pressure Drop Measurements [5] in 90° Inclined Tube Bundles

Tube Arrangement	Reynolds Number (Experiment)	CFD Simulation					Normalized Flow Resistance (Experiment), B	Error (= (A-B)/B)
		Inlet Velocity [m/s]	Velocity @ Mid Position [m/s]	Reynolds Number @ Mid Position	ΔP/ΔL @ Mid Position [Pa/m]	Normalized Flow Resistance (Eq. (8)), A		
In-line (Square) $\theta = 0^o$ (Cross flow) $T_{avg} = 27.8\ ^oC$ $\rho = 998.0\ kg/m^3$ $\beta = 0.650935$ (porosity) $D_h = 0.0103$ m $A_{channel} = 0.004083\ m^2$	4280	0.378993	0.382774	4322.5	6100.7	2936.7	2860	2.7%
	10200	0.893624	0.898639	10257.4	33733.0	6530.7	5410	20.7%
	19100	1.65586	1.66225	19174.1	90281.0	9449.1	8930	5.8%

Table 3: Verification for the Axial Hydraulic Resistance

Case	Inlet Velocity (Upstream)	Actual Velocity at the Mid Position in Porous Region	Estimated Reynolds No. in the Porous Region	Friction Loss Coefficient (f_z in Eq. (9))	Pressure Drop Ratio (ΔP/ΔL)	
					Simulation Result	Estimation* (Eq. (11))
1	0.12774 m/s	0.13191 m/s	4947.9	0.03984	11.145 Pa/m	11.081 Pa/m
2	0.41783 m/s	0.42703 m/s	16016.3	0.02846	83.592 Pa/m	82.931 Pa/m
3	0.71628 m/s	0.72964 m/s	27360.5	0.02482	209.861 Pa/m	211.215 Pa/m

* The estimated pressure drop ratios are calculated based on the actual velocity (u) in the porous region from the simulation result, which is not a superficial velocity.